

Cite this: *J. Mater. Chem.*, 2012, **22**, 10589

www.rsc.org/materials

PAPER

Diketopyrrolopyrrole-based oligomer modified TiO₂ nanorods for air-stable and all solution processed poly(3-hexylthiophene):TiO₂ bulk heterojunction inverted solar cell†

Hsueh-Chung Liao,^a Chia-Hsin Lee,^b Yi-Chen Ho,^a Meng-Huan Jao,^a Chieh-Ming Tsai,^a Chih-Min Chuang,^b Jing-Jong Shyue,^c Yang-Fang Chen^{*d} and Wei-Fang Su^{*a}

Received 17th January 2012, Accepted 19th March 2012

DOI: 10.1039/c2jm30334e

Diketopyrrolopyrrole-based oligomer was synthesized and used to modified TiO₂ nanorods. The surface modified TiO₂ was employed in the fabrication of air-stable and all solution processed poly(3-hexylthiophene):titanium dioxide nanorods (P3HT:TiO₂ nanorods) bulk heterojunction (BHJ) inverted solar cells. The oligomer (copolymerized 4,5-diaza-9,9'-spirobifluorene with diketopyrrolopyrrole (PZFDPP)) was synthesized by Stille coupling reaction. The PZFDPP was coated on TiO₂ nanorods by refluxing the TiO₂ nanorods in oligomer containing solution at low temperature (70 °C). A concentration gradient profile of polymer/nanocrystals (P3HT/TiO₂ nanorods) BHJ was observed for the first time by X-ray photoelectron spectroscopy (XPS) technique together with *in situ* ion sputtering, showing that the TiO₂-rich region and P3HT rich region are aggregated adjacent to electron transport layer (ETL) and hole transport layer (HTL) respectively. The obtained depth profile indicates the inverted device structure is more suitable for polymer/inorganic nanocrystals BHJ solar cells. Furthermore, instead of using an energy consuming process for ETL layer deposition, the PZFDPP modified TiO₂ nanorods were used to deposit the ETL layer by spin coating. The surface features and properties of deposited TiO₂ ETL that was coated by PZFDPP were systematically investigated. The developed photovoltaic device shows a promising power conversion efficiency (PCE) of 1.2% benefited from improved electron mobility in P3HT:TiO₂ BHJ film and across the ETL/active layer interfaces. Moreover, the device is extremely stable stored in ambient condition without encapsulation (less than 10% loss over 1000 h test). The results of this work demonstrate the successful development of highly efficient and air-stable polymer/inorganic nanocrystal hybrid BHJ inverted solar cells based on chemically modified nanocrystals which significantly extend the current knowledge of device fabrication.

Introduction

Polymer solar cells have attracted great attention due to their advantages of light weight, mechanical flexibility, ease of fabrication, and low cost. At present, the bulk heterojunction (BHJ) based on the intimate mixing of electron donor and electron

acceptor is the most promising device structure. The BHJ provides large interfaces for exciton dissociation and bi-continuous pathway for carrier transport. Efficiencies up to 4–5% have been achieved using the widely investigated poly(3-hexylthiophene) (P3HT) as electron donor and fullerene derivatives (PCBM) as electron acceptor.^{1,2} However, several issues regarding the usage of PCBM need to be addressed including cost, thermal stability, dielectric constant and electron mobility. An alternative polymer solar cell system involving the hybrid of conducting polymer (as electron donor) and inorganic nanocrystal (as electron acceptor) was thus developed, which is known as a hybrid BHJ solar cell. Various n-type nanocrystals have been successfully applied in the hybrid solar cell such as CdSe,^{3–6} TiO₂^{7–11} and ZnO.^{12–16} Particularly, TiO₂ nanocrystals have attracted significant interests considering the successful application in dye sensitized solar cells (DSSC). The low cost, environmental friendly and high thermal and physical stability all make TiO₂ a promising candidate in hybrid solar cell application.

^aDepartment of Materials Science and Engineering, National Taiwan University, No. 1, Sec. 4, Roosevelt Road, Taipei 10617, Taiwan. E-mail: suwf@ntu.edu.tw; Fax: +886 2 33664078; Tel: +886 2 33664078

^bInstitute of Nuclear Energy Research, No. 1000, Wenhua Rd., Longtan Township, Taoyuan County 32546, Taiwan

^cAcademia Sinica, No. 128, Academia Road, Section 2, Nankang, Taipei 115, Taiwan

^dDepartment of Physics, National Taiwan University, No. 1, Sec. 4, Roosevelt Road, Taipei 10617, Taiwan. E-mail: yfchen@phys.ntu.edu.tw; Fax: +886 2 33665125; Tel: +886 2 33665125

† Electronic supplementary information (ESI) available: Synthesis procedure and detailed characterization of oligomer PZFDPP. See DOI: 10.1039/c2jm30334e

Moreover, one dimensional TiO₂ nanorods with high aspect ratios provide a direct pathway for electron transport and can be synthesized by simple sol-gel method at low temperature.^{17,18} As a result, the hybrid of polymer:TiO₂ nanorods has been widely investigated.⁷⁻¹¹

Typically, the BHJ solar cell is implemented into a conventional device structure in which the electron and hole are collected by metal electrode and transparent electrode respectively. However, there are some concerns of such structure as summarized in the following: (1) the typically used acidic hole transporting layer, poly(3,4-ethylenedioxythiophene):poly(styrenesulfonate) (PEDOT:PSS), harmfully etch the substrates indium tin oxide (ITO) thus significantly degrading the device performance,¹⁹⁻²¹ (2) the metal anode with low work function such as Al results in the formation of oxides thus extensive hermetic encapsulation for preventing the exposure to oxygen or moisture is usually required, and (3) instead of a uniform distribution of the blending materials, a vertical composition gradient in which the electron donor rich domains are close to the cathode and the electron acceptor rich domains are close to the anode was found in the BHJ film.²²⁻²⁵ Such a gradient profile is obviously not desired for the operation of efficient charge transport in conventional devices. Therefore, the inverted device structure operated in the reverse way (electron and hole are collected from transparent electrode and metal electrode respectively) was then developed. It exhibits significant device stability and more compatible gradient profile that facilitates the electron and hole transport.²⁶⁻³⁹ One of the crucial factors for achieving high efficiency in inverted devices is choosing the materials for the electron transporting layer (ETL) and hole transporting layer (HTL). A lot of investigations have been carried out based on various carrier transporting materials such as CsCO₃,^{26,27} TiO₂,^{25,28-33} ZnO³⁴⁻³⁹ for electron transport and V₂O₅,^{26,27,33,39} WO₃,³⁸ MoO₃,^{28,36,37} PEDOT:PSS^{25,30,35,40-42} for hole transport. While the inverted structure based on P3HT:PCBM BHJ has been extensively investigated,²⁶⁻³⁹ to our knowledge there is no study reporting the inverted structure with respect to polymer:inorganic nanocrystals hybrid BHJ solar cell to date. The present study for the first time demonstrates the examination of the vertical phase separation of polymer P3HT and inorganic nanocrystals TiO₂ and furthermore establishes an inverted solar cell based on the P3HT:TiO₂ nanorods BHJ. TiO₂ and PEDOT:PSS were adopted as the ETL and HTL respectively. Sandwiched between is the P3HT:TiO₂ BHJ which constructs the ITO/TiO₂/P3HT:TiO₂/PEDOT:PSS/Ag device structure as shown in Fig. 1a and the energy diagram of each component as shown in Fig. 1b.

TiO₂ has been extensively adopted as an ETL in DSSC system and inverted P3HT:PCBM solar cell.²⁶⁻³⁹ However, the deposition of a TiO₂ layer typically includes complex and energy-consuming processes such as sintering processes higher than 450 °C,^{25,29,32,33} electrospinning,⁴³ electrochemical anodization,³¹ etc. Most of them have the similar purposes of densifying the TiO₂ film or creating mesoporous or ordered nanostructure for accommodating dye or polymer molecules. However, the strict requirement of those processing conditions for depositing the TiO₂ layer is not suitable for roll-to-roll processing on flexible substrate. In the present study, we develop a solution and annealing-free process to deposit the

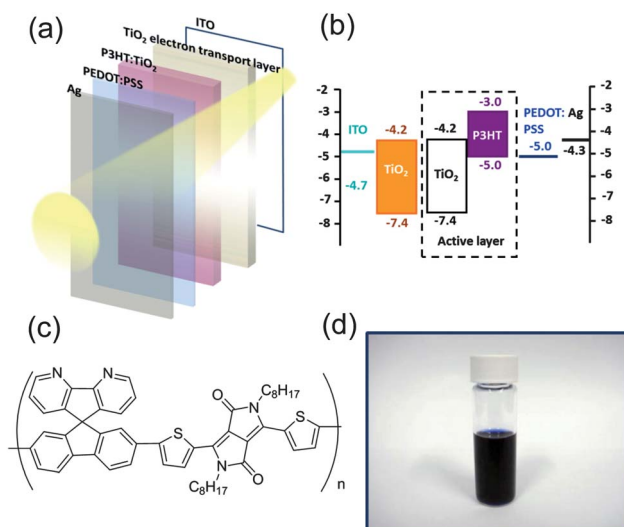


Fig. 1 (a) Schematic representation of inverted device structure including Ag/PEDOT:PSS/P3HT:TiO₂/TiO₂ ETL/ITO layers from the top down. (b) Energy diagram of each layer corresponding to the inverted device structure. (c) Molecular structure of oligomer PZFDPP. The molecular weight is about 3000, indicating the number of repeating units of 5 ($n = 5$). (d) Picture of PZFDPP modified TiO₂ nanorods pyridine solution.

TiO₂ film by directly spin coating the solution of TiO₂ nanorods. In order to improve the compatibility between the P3HT:TiO₂ hybrid film and TiO₂ ETL film, the 4,5-diaza-9,9'-spirobifluorene copolymerized with diketopyrrolopyrrole (PZFDPP) was used as a surface modifier. The modifier was placed on the TiO₂ nanorods by refluxing the TiO₂ nanorods in the modifier containing pyridine solution at low temperature (~70 °C). The molecular structure of PZFDPP with number average molecular weight ($M_n = 1587$), weight average molecular weight ($M_w = 2015$) and polydispersity index (PDI = 1.27) is shown in Fig. 1c. Its detailed synthesis procedure and characterization are described in the supplementary information.† The electron deficient unit (DPP) with pyridine-like moiety is expected as an electron transporting linker on the surface of TiO₂ nanorods. The PZFDPP modified TiO₂ nanorods pyridine solution (as pictured in Fig. 1d) was used in both the deposition of the TiO₂ ETL layer and preparation of the P3HT:TiO₂-PZFDPP hybrid solution. The surface properties of TiO₂ ETL layer was systematically studied with respect to the different surface modifiers either small molecular pyridine (TiO₂-pyridine) or oligomer PZFDPP (TiO₂-PZFDPP). Additionally, the PEDOT:PSS was adopted as the hole transport layer (HTL) owing to its excellent oxygen-blocking ability which leads to the improvement of device stability.⁴⁰ The inverted device structure based on this modified P3HT:TiO₂ hybrid material exhibits promising power conversion efficiency (PCE) of 1.2%. Moreover, the device reveals excellent stability stored in air without encapsulation. The present work demonstrates the employment of oligomer modified TiO₂ nanorods in a highly efficient and air-stable inverted polymer/nanocrystal hybrid BHJ solar cell. The developed annealing-free and all solution process is of significance for extending the current device fabrication technology.

Experimental details

Materials

The TiO₂ nanorods with high aspect ratio and anatase phase were synthesized according to previous work.^{7–11} The as-synthesized TiO₂ nanorods capped with oleic acid were dissolved in pyridine (10 mg ml⁻¹) and refluxed at 70 °C under N₂ flow for one day, allowing for comprehensive ligand exchange and yielding the pyridine capped TiO₂ nanorod (TiO₂-pyridine). The oligomer PZFDPP (see supplementary information for details†) was then used to modify the surface of TiO₂ nanorods by adding 3 mg PZFDPP into 20 ml TiO₂-pyridine solution and refluxing at 70 °C under N₂ flow for one day, yielding the PZFDPP capped TiO₂ nanorods (TiO₂-PZFDPP). The hexane (95% Acros) was added into the TiO₂-pyridine and TiO₂-PZFDPP solution followed by centrifugation in order to precipitate the TiO₂ nanorods and remove the non-absorbed surface ligands. The modified TiO₂ nanorods were used both in the deposition of the TiO₂ ETL and the preparation of the P3HT:TiO₂ hybrid solution.

Device fabrication

We used a layer-by-layer deposition and all-solution process to fabricate the photovoltaic device in an inverted structure. All the layers deposited from each solution were performed in air. For the inverted device fabrication, the transparent electrode ITO (Merck) with a sheet resistant of 15 Ω was ultrasonically cleaned by a series of solvent (ammonia/H₂O₂/deionized water, methanol, isopropanol) followed by oxygen plasma treatment. The modified TiO₂ nanorod solution with a concentration of 30 mg ml⁻¹ in pyridine was prepared and spin cast on the indium tin oxide (ITO, Merck) as the ETL. Afterwards, a thin active layer consisting of P3HT:TiO₂ nanorods hybrid was deposited on the ETL layer. The solution of P3HT:TiO₂ was prepared in a 47 : 53 wt/wt ratio in a co-solvent system (chlorobenzene, pyridine, dichloromethane, chloroform).⁷ Subsequently, the hole transporting layer of PEDOT:PSS (Baytron P, 4083) was dissolved in ethanol in 1 : 1 vol/vol ratio and spin coated on the active layer. Finally, the metal electrode Ag was deposited by thermal evaporation under vacuum at 3 × 10⁻⁶ Torr to complete the device fabrication (Fig. 1a) with an area of 0.06 cm². The electron mobility measurement was obtained from an electron-only device. Namely, the deposited layer for analysis was sandwiched between two Al electrodes. For the device fabrication in forward structure, the detailed fabrication process can be found elsewhere.⁷ In short, the PEDOT:PSS was first spin coated on the ITO substrate followed by baking at 120 °C for 10 min. Afterwards, the P3HT:TiO₂ hybrid solution was spin coated on the PEDOT:PSS. An additional layer of TiO₂ nanorods was sandwiched between the P3HT:TiO₂ active layer and the upper cathode Al (deposited from thermal evaporation), leading to the forward device structure of ITO/PEDOT:PSS/P3HT:TiO₂/TiO₂/Al.

Characterization

The depth profile of the hybrid film was performed using *in situ* sputtering during XPS measurement which was recorded from PHI 5000 VersaProbe (ULVAC-PHI, Chigasaki, Japan) system

with a microfocused (100 μm, 25 W) Al X-ray beam. The details of the system setup can be found elsewhere.⁴⁴ In short, the Ar⁺ and C60⁺ ion beams were obtained from Ar⁺ ion source (FIG-5CE) and C60⁺ ion source (IOG C60-10, Ionoptika, Chandler's Ford, U.K.) respectively. The measurement was conducted at the pressure of <1 × 10⁻⁷ Pa by evacuating the main chamber using turbomolecular and ion-getter pumps. The UV-Vis absorption spectrum (PerkinElmer Lambda 35) was used to determine the absorption amount of PZFDPP on TiO₂ nanorods. The SEM images of TiO₂ ETL surface features were obtained from JOEL JEM-1230 microscope operating at 100 keV. The topographic observation of TiO₂ ETL film was analyzed by AFM (Digital Instruments, Nanoscopes III). The water contact angle was measured by the contact angle instrument (Sindatek Model 100SB) by using water droplets with a volume of 1–4 μl. Ten measurements were performed on each sample and the average plus standard deviation of the angles were recorded. The current–voltage measurement of SCLC and PCE was performed under air atmosphere using Keithley 2400 source meter. The photocurrent of the photovoltaic devices was characterized under A.M. 1.5 radiation (100 mW cm⁻²) using a solar simulator source (Newport Inc.). For the device stability test, the as-fabricated devices were stored under air atmosphere without encapsulation (room temperature of 26 °C and relative humidity between 40% and 60%).

Results and discussion

The composition distribution of the P3HT:TiO₂ (47 : 53 by wt.) hybrid thin film along the vertical direction would be varied owing to the large difference of density between polymer (P3HT, $d \approx 1.1 \text{ g cm}^{-3}$) and nanocrystals (TiO₂, $d \approx 4 \text{ g cm}^{-3}$). We have examined the composition distribution carefully using XPS technique. The XPS depth profiling accompanied by mixed-ion sputtering (a mixture of C₆₀⁺ ions and Ar⁺ ions) is a powerful technique to probe organic electronic devices with preserved chemical states and steady sputtering rate.⁴⁴ By using the mixture of ions, the vertical composition profile of P3HT:TiO₂ BHJ solar cell in the inverted structure can be probed as shown in Fig. 2. The elements we characterized included Ag, C, Ti, O, In, and S (resolved to thiophene and sulfonate). Therefore, from the variation of the atomic concentration with sputtering time, the profile clearly shows respective layers corresponding to the fabricated device structure (Fig. 1a), *i.e.* Ag anode showed before 80 min, HTL PEDOT:PSS was between 80 min and 150 min, P3HT:TiO₂ hybrid active layer was between 150 min and 300 min, TiO₂ ETL layer was between 300 min and 600 min, and then ended with transparent electrode ITO. Additionally, corresponding to the film thickness obtained from α -stepper measurement, the sputtering rate can be calibrated to 0.95 nm min⁻¹. In order to examine the composition gradient in the P3HT:TiO₂ BHJ layer, the atomic concentration of thiophene (characteristic of P3HT) was divided by Ti (characteristic of TiO₂) as shown in the inset of Fig. 2. It can be clearly observed that the mixture of P3HT and TiO₂ shows a concentration gradient instead of homogeneous distribution along the vertical direction. In other words, during the spin coating process of hybrid P3HT:TiO₂ solution, the TiO₂ nanorods tend to sink down to the bottom while the P3HT stays relatively near the top,

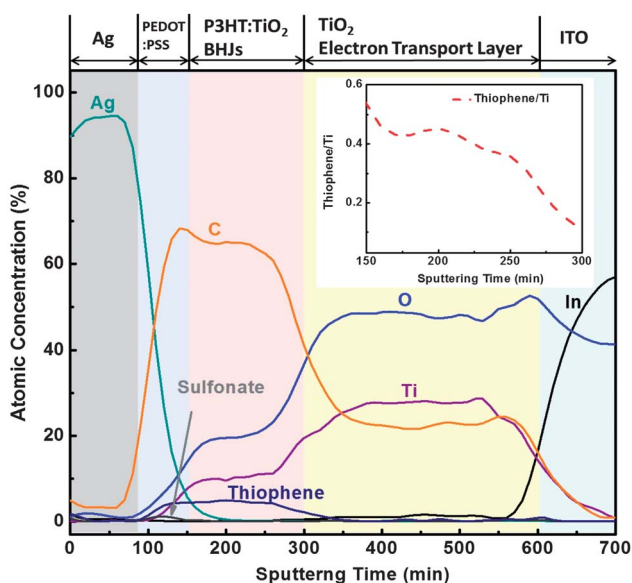


Fig. 2 XPS depth profile of inverted device with recorded elements of Ag, S (resolved to sulfonate and thiophene), Ti, O, In, and C. The inset shows the atomic concentration ratio of thiophene/Ti within the sputtering time of 150 min and 300 min, which is resolved to be the P3HT:TiO₂ BHJ layer.

leading to the decreased thiophene/Ti ratio with sputter time. The obtained concentration gradient indicates that the inverted device architecture is more favorable for efficient charge collection than that of forward device structure.

For the inverted device structure developed in the present study, the TiO₂ ETL was deposited by spin coating the TiO₂ nanorods solution (anatase phase).^{7–11} It has been demonstrated in our previous work that the as-capped surface ligand oleic acid (OA) on TiO₂ nanorods can be replaced by refluxing the TiO₂ nanorods in surface modifiers (small molecules or oligomers) containing pyridine solution.^{7,8} Pyridine is a commonly used small molecule for ligand exchange of surfactant on inorganic nanocrystals through the lone pair electron of nitrogen. For further improving the electron transport of deposited TiO₂ ETL layer and the wet ability for ease of processing of P3HT:TiO₂ hybrid solution on the top of the TiO₂ ETL layer, oligomer PZFDPP was synthesized and used to modify the surface of TiO₂ nanorods. The typical high temperature sintering process for TiO₂ layer (>450 °C) was thus excluded. It has been extensively demonstrated that the chemical modification of TiO₂ surface is usually through the carboxylic functional group COOH. Herein, the oligomer PZFDPP was designed to modify the surface of TiO₂ nanorods *via* the pyridine-like moiety (Fig. 1c). Therefore the adsorption amount of PZFDPP on TiO₂ nanorods needs to be carefully determined. UV-Vis absorption spectrum and the Beer's law were used for quantitative determination by focusing on the absorbance of PZFDPP ranged from 450 to 700 nm. Fig. 3a shows the absorption spectrum of pristine PZFDPP dissolved in pyridine with different concentrations. The calibration curve can hence be obtained by linearly fitting the absorbance centered at wavelength of 580 nm *versus* the concentration of oligomer as plotted in Fig. 3b. We added hexane into TiO₂-PZFDPP followed by centrifugation in order to remove the un-

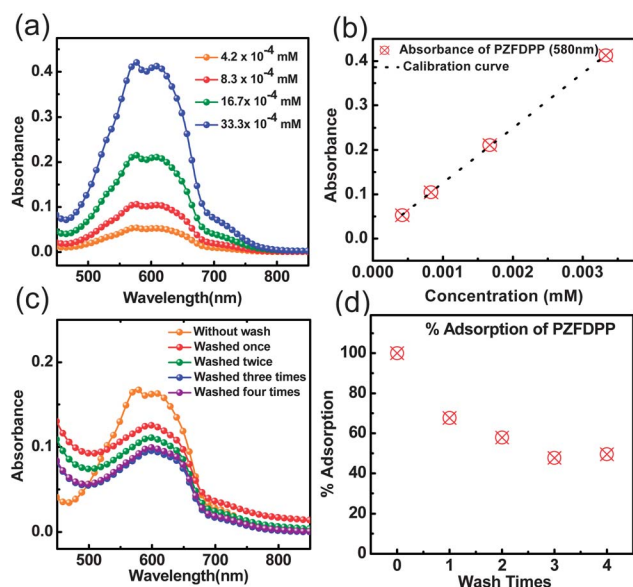


Fig. 3 Determination of the adsorption amount of oligomer PZFDPP on TiO₂ nanorods. (a) UV-Vis absorption spectrum of PZFDPP dissolved in pyridine with different concentrations. (b) Calibration curve of PZFDPP absorbance versus concentration. (c) UV-Vis absorption spectrum of PZFDPP modified TiO₂ nanorods dissolved in pyridine with different times of washing and centrifugation. (d) Percentage of adsorption of PZFDPP on TiO₂ nanorods with respect to that of TiO₂-PZFDPP solution without centrifugation.

adsorbed oligomer PZFDPP. Fig. 3c shows the absorption spectrum of TiO₂-PZFDPP nanorods dissolved in pyridine. The TiO₂-PZFDPP nanorods have been washed by hexane for different times. We can observe that the absorbance of TiO₂-PZFDPP was decreased after the first hexane washing and then the absorbance remained almost the same after three washings. It indicates that the un-adsorbed PZFDPP on TiO₂ can be completely removed by repeated hexane washing and centrifuging and a considerable amount of PZFDPP is tightly bonded to the TiO₂ nanorods. Corresponding to the calibration curve plotted in Fig. 3b, the amount of adsorbed oligomer can be calculated to be 9.1×10^{-12} mole cm⁻², which is in the same order as, and even larger than that of molecules with carboxylic functional groups reported in the literature.⁷

Fig. 4a and 4b show the scanning electron microscope (SEM) images of surface features of TiO₂ ETL films spin coated from TiO₂-pyridine and TiO₂-PZFDPP respectively. The ETL film of TiO₂-pyridine presents nanometer-sized particles individually distributing over the thin film. It indicates that during spin coating, the nanorods stick to each other and construct the nano-scale particulate morphology. Such particulate nanostructure is about 10–15 nm in diameter. Hence it can be deduced that several nanorods are bunched together and stand along the vertical direction (the individual nanorod is on average 4–5 nm in diameter and 35 nm in length⁸), leading to the observed nanometer-sized particulate nanostructure. Therefore, such standing bunches could be beneficial for carrier transport considering the efficient electron collecting from the active layer to the nanorods tip of particulate nanostructure, followed by transport toward the electrode through direct pathway. On the other hand, the

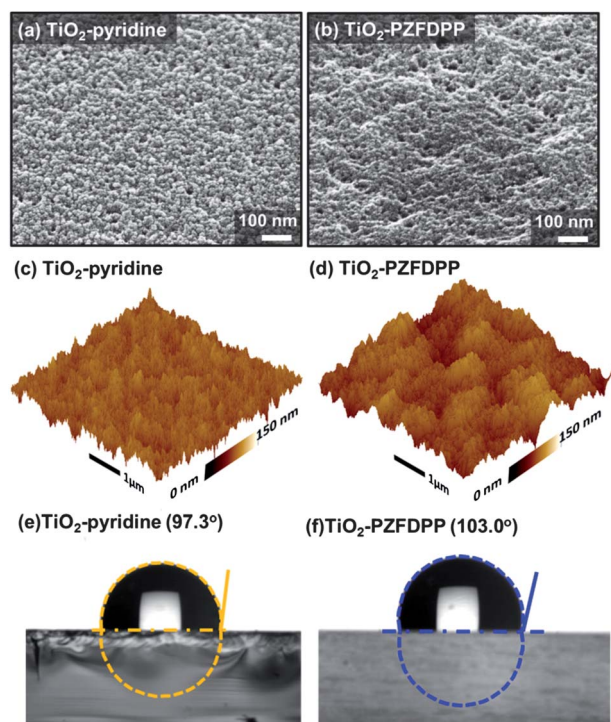


Fig. 4 Analysis of surface property of TiO₂ ETL spin coated from TiO₂ nanorods solution with respect to different surface modifiers. (a, b) SEM images, (c, d) AFM images (e, f) contact angle measurement of ETL surface of TiO₂-pyridine and TiO₂-PZFDPP respectively.

ETL spin coated from oligomer modified TiO₂ nanorods (TiO₂-PZFDPP) presents a very different morphology to that of TiO₂-pyridine film. The nanoparticles are no longer individually separated. Instead, some nanoparticles gather to form larger agglomerations. Furthermore, it can be observed that the agglomerations or the particles are coated by a soft material of oligomer PZFDPP. The results suggest that the oligomer modification would significantly vary the morphology of the self-organized TiO₂ film during spin coating, which would directly affect the accommodating ability for the P3HT:TiO₂ hybrid. The atomic force microscope (AFM) images shown in Fig. 4c and 4d of TiO₂ ETL films spin coated from TiO₂-pyridine and TiO₂-PZFDPP respectively are further supportive in observing the topography of the TiO₂ film. The TiO₂-pyridine film exhibits finer surface features with needle-like structures distributed over the thin film. However, the TiO₂-PZFDPP film shows a topography of lump shapes of agglomerations which are resulted from the assembled needle-like structure and the oligomer coated surface. The water contact angle measurements of the TiO₂-pyridine and TiO₂-PZFDPP films were used to examine its wetting ability as pictured in Fig. 4e and 4f respectively. The TiO₂-pyridine film exhibits hydrophobic properties (contact angle = 97.0°) that can be attributed to the adsorption of pyridine on TiO₂ nanorods through the unshared electron of nitrogen atom. Moreover, the contact angle of oligomer modified TiO₂ film further increases from 97.0° to 103.0° compared to that of pyridine capped TiO₂ film. The increased hydrophobicity can be attributed to two reasons: (1) the rougher surface features of TiO₂-PZFDPP film (root mean square roughness = 31.1 nm)

compared to that spin coated from pyridine modified TiO₂ nanorod (root mean square roughness = 18.7 nm), and (2) the intrinsic hydrophobicity of the oligomer PZFDPP coated on the surface of TiO₂. Owing to the hydrophobic solvents used in the preparation of P3HT:TiO₂ hybrid (chlorobenzene, chloroform, dichloromethane, and pyridine), the enhanced hydrophobicity of the ETL layer can help the flow and the spread of the active layer solution spin coating over the ETL layer.⁴⁵ Consequently, it suggests that the oligomer modification can facilitate the accommodating of the P3HT:TiO₂ hybrid layer in the three dimensional nanostructure of TiO₂ ETL film constructed by TiO₂ nanorods. The improved ETL/active layer interface properties are hence expected to reduce the recombination of charge carriers at the interface and improve the device performance.

The electron transporting properties of thin films were characterized by employing the space carrier limited current (SCLC) method. The electron only device was fabricated by sandwiching the thin film between two Al electrodes. Therefore, when the current is SCLC, the current density follows the Mott–Gurney law based on the trap-free assumption:⁴⁶

$$J = \frac{9}{8} \epsilon_0 \epsilon \mu \frac{(V_{\text{app}} - V_{\text{bi}})^2}{L^3}$$

where ϵ_0 is the permittivity of free space, ϵ is the dielectric constant of the materials, μ is carrier mobility, V_{app} is the applied

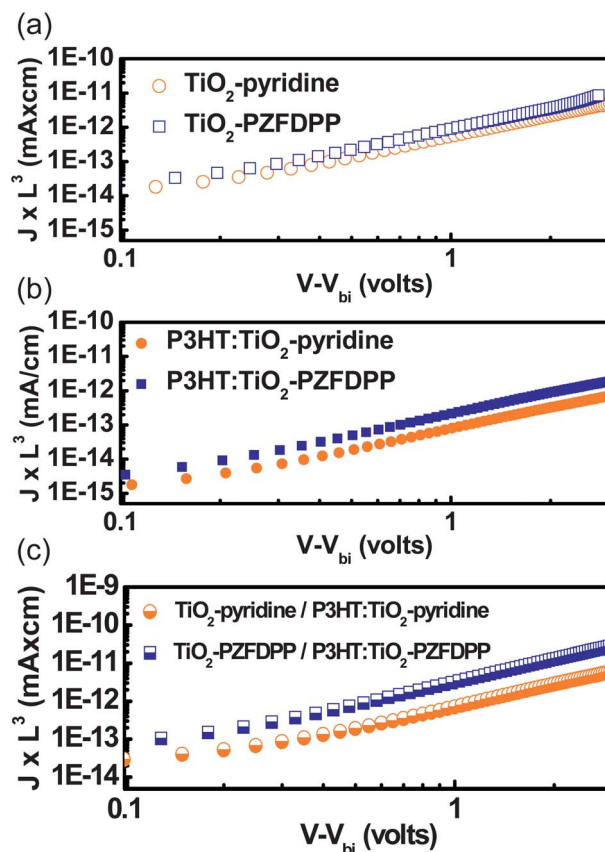


Fig. 5 Electron mobility obtained from SCLC measurement with respect to different surface modifier: (a) TiO₂ electron transport layer, (b) P3HT:TiO₂ hybrid active layer and (c) TiO₂ ETL + P3HT:TiO₂ bi-layer.

voltage across device, V_{bi} is the built-in voltage, and L is the thickness of the film. Hence, the electron mobility can be obtained by plotting the current *versus* voltage as shown in Fig. 5a, 5b and 5c for ETL, active layer and ETL + active layer bi-layer respectively with respect to different surface modifiers. It is noteworthy that the different molecule modified TiO₂ nanorods solution used in the ETL deposition was also respectively used in the mixture of P3HT:TiO₂. The fitting results of oligomer PZFDPP modified TiO₂ in comparison with those of pyridine modified TiO₂ were summarized in Table 1. The mobility of ETL fabricated from either TiO₂-pyridine or TiO₂-PZFDPP is similar, indicating that the transporting property of the TiO₂ nanorod remains unchanged after oligomer modification. However, the mobility of active layer fabricated from oligomer modified TiO₂-PZFDPP blended with P3HT shows three times enhancement as compared to that of TiO₂-pyridine blended with P3HT (from $1.6 \times 10^{-5} \text{ cm}^2 \text{ V}^{-1} \text{ s}^{-1}$ to $4.8 \times 10^{-5} \text{ cm}^2 \text{ V}^{-1} \text{ s}^{-1}$). Owing to the similarly intrinsic property of electron transport between TiO₂-pyridine and TiO₂-PZFDPP nanorods, the improved electron mobility can be attributed to the different nanostructure of TiO₂ nanorods dispersed in P3HT matrix using different surface modified TiO₂ nanorods. It has been demonstrated that the surface modification of TiO₂ nanorods by pyridine molecules led to aggregation of the nanorods.⁷ On the other hand, the TiO₂ nanorods modified by large molecule of PZFDPP exhibits better dispersity and compatibility with P3HT to form P3HT:TiO₂ bulk heterojunction. As a consequence, the well-dispersed TiO₂-PZFDPP nanorods construct a closer interconnect and more continuous pathway for carrier transport. Moreover, considering the bilayer of ETL and active layer (Fig. 5c), the electron mobility is considerably enhanced by nearly five times from $1.4 \times 10^{-4} \text{ cm}^2 \text{ V}^{-1} \text{ s}^{-1}$ to $6.5 \times 10^{-4} \text{ cm}^2 \text{ V}^{-1} \text{ s}^{-1}$ after using the PZFDPP modified TiO₂ nanorods. In addition to the modified nanostructure in bulk heterojunction, the improved interface properties between the ETL and the active layer also account for the enhancement in mobility. The distinctive surface feature of ETL spin coated from TiO₂-PZFDPP described above leads to the improved contact and thus promoted electron mobility across the ETL/active layer interface.

The current density–voltage (J–V) curves of P3HT:TiO₂ BHJ solar cells in inverted structure are plotted in Fig. 6 for different surface modifier system. The performance characteristics obtained from the J–V curves are summarized in Table 1. The device based on the pyridine modified system exhibits a PCE of 0.6% with $V_{oc} = 0.64 \text{ V}$, $J_{sc} = 1.5 \text{ mA cm}^{-2}$ and FF = 52%. By using the oligomer PZFDPP for the surface modification of TiO₂ nanocrystals, a significant improvement by 2 times was furthermore achieved showing the promising PCE of 1.2% ($V_{oc} = 0.62 \text{ V}$, $J_{sc} = 3.8 \text{ mA cm}^{-2}$ and FF = 52%). As discussed

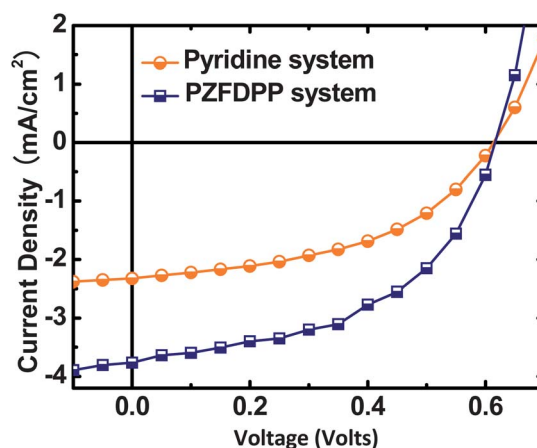


Fig. 6 Photocurrent–voltage characteristics of inverted photovoltaic devices based on P3HT:TiO₂ BHJ using different surface modifier (under A.M. 1.5 illumination, 100 mW cm^{-2}).

above, the considerable improvement by oligomer modification can be attributed to the increased electron mobility both inside the BHJ film (resulted from varied three dimensional nanostructure) and across the interface of the ETL/active layer. For the device stability test, the devices fabricated using PZFDPP modified TiO₂ nanorods were compared with respect to forward and inverted device structure as shown in Fig. 7, with initial PCE of 0.72% and 0.95% respectively. Both devices were stored and characterized in air under ambient condition without encapsulation. It can be clearly observed that the device in forward structure shows dramatically decreased performance

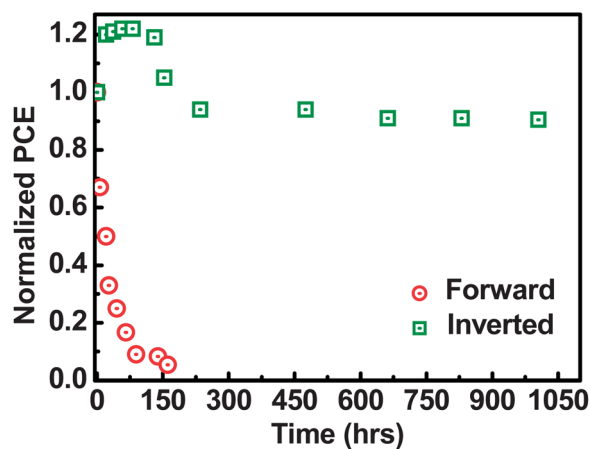


Fig. 7 Device stability test based on P3HT:TiO₂ hybrid BHJ of forward and inverted solar cells. Both the devices were stored in air without encapsulation and the PCE measurement was also performed in air.

Table 1 Summary of electron mobility of different layers (ETL, active layer, ETL + active layer) and the device performance characteristics (V_{oc} , J_{sc} , FF, PCE) with respect to different surface modifier system

System	μ_e (ETL) ($\text{cm}^2 \text{ V}^{-1} \text{ s}^{-1}$)	μ_e (active layer) ($\text{cm}^2 \text{ V}^{-1} \text{ s}^{-1}$)	μ_e (ETL + active layer) ($\text{cm}^2 \text{ V}^{-1} \text{ s}^{-1}$)	V_{oc} (V)	J_{sc} (mA cm^{-2})	FF (%)	PCE (%)
Pyridine	$1.1 \pm 0.5 \times 10^{-4}$	$1.6 \pm 0.5 \times 10^{-5}$	$1.4 \pm 0.6 \times 10^{-4}$	0.64	1.5	52	0.6 ± 0.18
PZFDPP	$1.8 \pm 0.3 \times 10^{-4}$	$4.8 \pm 0.4 \times 10^{-5}$	$6.5 \pm 0.4 \times 10^{-4}$	0.62	3.8	52	1.2 ± 0.13

(<10%) within 150 h storage. The considerably dropped PCE can be attributed to the oxidation of cathode Al and the etched anode ITO by acidic PEDOT:PSS when the device was exposed to moister condition. On the other hand, the device in inverted structure exhibits extremely stable performance in air with less than 10% loss over 1000 h (compared to the initial device performance as fabricated). Note that the PCE in inverted structure gradually increases for the first 150 h (by nearly 20%) which is typically observed in the inverted device structure with Ag electrode and can be attributed to the oxidation of Ag.³⁴ Briefly speaking, oxygen in air tends to diffuse toward the metal/organic interfaces of the as-fabricated device stored under ambient condition. Consequently, this leads to the formation of silver oxide which shows larger work function of -5.0 eV as compared with that of Ag (-4.3 eV). The work function shift leads to well matched electrical coherence between the HOMO of PSDOT:PSS (-5.1 eV) and the effective work function of anode (-5.0 eV). Therefore, the improved carrier collection at the metal/organic interfaces reduces the recombination and hence enhanced the PCE for the first 150 h. In short, the implement of P3HT:TiO₂ BHJ solar cell into inverted device structure leads to the considerably stable device performance without expensive and complicated encapsulation which is a promising advance in the technology of device fabrication.

Conclusions

In summary, an inverted solar cell of P3HT:TiO₂ BHJ using oligomer PZFDPP modified TiO₂ nanorods was developed based on all-solution and annealing free fabrication process. The depth profile analysis reveals a concentration gradient exists in the BHJ of P3HT:TiO₂ hybrid, suggesting an inverted device structure is suitable for achieving high PCE. The TiO₂ ETL can be fabricated by directly spin coating TiO₂ nanorods solution without energy-consuming sintering process. Furthermore, employing chemical modification of TiO₂ nanorods by oligomer PZFDPP results in (1) variation of surface features of deposited TiO₂ ETL layer, (2) increased hydrophobicity of TiO₂ ETL layer, (3) better dispersity of TiO₂ nanorods in P3HT matrix, (4) enhanced electron transport in both active layer of P3HT:TiO₂ BHJ and interface layer between ETL and active layer. Thus an enhanced device performance is obtained as compared to the system with pyridine modified TiO₂ nanorods. A promising PCE of 1.2% was achieved using PZFDPP modified TiO₂ nanorods. Furthermore, the device exhibits extremely stable PCEs upon storage in air without any complicated encapsulation (less than 10% loss over 1000 h). This study points toward a useful direction for chemical modification of inorganic nanocrystal and developing low-cost polymer solar cells with high efficiency and stability.

Acknowledgements

Financial support obtained from National Science Council of Taiwan (99-2120-M-002-011, 100-2120-M-002-00, 101-3113-E-002-010) and Institute of Nuclear Energy Research (Projects 10020011NER048) are highly appreciated.

Notes and references

- 1 G. Li, V. Shrotriya, J. Huang, Y. Yao, T. Moriarty, K. Emery and Y. Yang, *Nat. Mater.*, 2005, **4**, 864.
- 2 W. Ma, C. Yang, X. Gong, K. Lee and A. J. Heeger, *Adv. Funct. Mater.*, 2005, **15**, 1617.
- 3 W. U. Huynh, J. J. Dittmer and A. P. Alivisatos, *Science*, 2002, **295**, 2425.
- 4 L. Han, D. Qin, X. Jiang, Y. Liu, L. Wang, J. Chen and Y. Cao, *Nanotechnology*, 2006, **17**, 4736.
- 5 B. Sun and N. C. Greenham, *Phys. Chem. Chem. Phys.*, 2006, **8**, 3557.
- 6 B. Sun, H. J. Snaith, A. S. Dhoot, S. Westenhoff and N. C. Greenham, *J. Appl. Phys.*, 2005, **97**, 014914.
- 7 Y. C. Huang, J. H. Hsu, Y. C. Liao, W. C. Yen, S. S. Li, S. T. Lin, C. W. Chen and W. F. Su, *J. Mater. Chem.*, 2011, **21**, 4450.
- 8 Y. Y. Lin, T. H. Chu, S. S. Li, C. H. Chuang, C. H. Chang, W. F. Su, C. P. Chang, M. W. Chu and C. W. Chen, *J. Am. Chem. Soc.*, 2009, **131**, 3644.
- 9 C. H. Chuang, Y. Y. Lin, Y. H. Tseng, T. H. Chu, C. C. Lin, W. F. Su and C. W. Chen, *J. Phys. Chem. C*, 2010, **114**, 18717.
- 10 Y. Y. Lin, T. H. Chu, C. W. Chen and W. F. Su, *Appl. Phys. Lett.*, 2008, **92**, 053312.
- 11 M. C. Wu, H. H. Lo, H. C. Liao, S. Chen, Y. Y. Lin, W. C. Yen, T. W. Zeng, Y. F. Chen, C. W. Chen and W. F. Su, *Sol. Energy Mater. Sol. Cells*, 2009, **93**, 869.
- 12 P. Ravirajan, A. M. Peiró, M. K. Nazeeruddin, M. Graetzel, D. D. C. Bradley, J. R. Durrant and J. Nelson, *J. Phys. Chem. B*, 2006, **110**, 7635.
- 13 H. M. P. Wong, P. Wang, A. Abrusci, M. Svensson, M. R. Andersson and N. C. Greenham, *J. Phys. Chem. C*, 2007, **111**, 5244.
- 14 W. J. E. Beek, L. H. Sloff, M. M. Wienk, J. M. Kroon and R. A. J. Janssen, *Adv. Funct. Mater.*, 2005, **15**, 1703.
- 15 W. J. E. Beek, M. M. Wienk and R. A. J. Janssen, *Adv. Mater.*, 2004, **16**, 1009.
- 16 S. D. Oosterhout, M. M. Wienk, M. Al-Hashimi, M. Heeney and R. A. J. Janssen, *J. Phys. Chem. C*, 2011, **115**, 18901.
- 17 P. D. Cozzoli, A. Kornowski and H. Weller, *J. Am. Chem. Soc.*, 2003, **125**, 14539.
- 18 T. W. Zeng, Y. Y. Lin, H. H. Lo, C. W. Chen, C. H. Chen, S. C. Liou, H. Y. Huang and W. F. Su, *Nanotechnology*, 2006, **17**, 5387.
- 19 A. Watanabe and A. Kasuya, *Thin Solid Films*, 2005, **483**, 358.
- 20 M. P. de Jong, L. J. van Ijzendoorn and M. J. Ad. Voigt, *Appl. Phys. Lett.*, 2000, **77**, 2255.
- 21 Y. Sahin, S. Alem, R. de Bettingnies and J. M. Nunzi, *Thin Solid Films*, 2005, **476**, 340.
- 22 H. Cheun, J. D. Berrigan, Y. Zhou, M. Fenoll, J. Shim, C. Fuentes-Hernandez, K. H. Sandhageb and B. Kippelen, *Energy Environ. Sci.*, 2011, **4**, 3456.
- 23 M. Campoy-Quiles, T. Ferenczi, T. Agostinelli, P. G. Etchegoin, Y. Kim, T. D. Anthopoulos, P. N. Stavrinou, D. D. C. Bradley and J. Nelson, *Nat. Mater.*, 2008, **7**, 158.
- 24 C. W. Liang, W. F. Su and Li Yi Wang, *Appl. Phys. Lett.*, 2009, **95**.
- 25 M. N. M. Glatthaar, B. Zimmermann, P. Lewer, M. Riede, A. Hinsch and J. Luther, *Thin Solid Films*, 2005, **491**, 298.
- 26 G. Li, C. W. Chu, V. Shrotriya, J. Huang and Y. Yang, *Appl. Phys. Lett.*, 2006, **88**, 253503.
- 27 H. H. Liao, L. M. Chen, Z. Xu, G. Li and Y. Yang, *Appl. Phys. Lett.*, 2008, **92**, 173303.
- 28 L. Shen, Y. Xu, X. D. Zhang, F. X. Meng, S. P. Ruan and W. Y. Chen, *Sol. Energy Mater. Sol. Cells*, 2010, **94**, 2451.
- 29 W. H. Baek, I. Seo, T. S. Yoon, H. H. Lee, C. M. Yun and Y. S. Kim, *Sol. Energy Mater. Sol. Cells*, 2009, **93**, 1587.
- 30 C. Waldauf, M. Morana, P. Denk, P. Schilinsky, K. Coakley, S. A. Choulis and C. J. Brabec, *Appl. Phys. Lett.*, 2006, **89**, 233517.
- 31 G. K. Mor, K. Shankar, M. Paulose, O. K. Varghese and C. A. Grimes, *Appl. Phys. Lett.*, 2007, **91**, 152111.
- 32 C. Y. Li, T. C. Wen, T. H. Lee, T. F. Guo, J. C. A. Huang, Y. C. Lin and Y. J. Hsu, *J. Mater. Chem.*, 2009, **19**, 1643.
- 33 B. Y. Yu, A. Tsai, S. P. Tsai, K. T. Wong, Y. Yang, C. W. Chu and J. J. Shyue, *Nanotechnology*, 2008, **19**, 255202.
- 34 M. S. White, D. C. Olson, S. E. Shaheen, N. Kopidakis and D. S. Ginley, *Appl. Phys. Lett.*, 2006, **89**, 143517.

-
- 35 S. K. Hau, H. L. Yip, N. S. Baek, J. Zou, K. O'Malley and A. K. Y. Jen, *Appl. Phys. Lett.*, 2008, **92**, 253301.
- 36 Z. Y. Hua, J. J. Zhang, Y. Liu, Z. H. Hao, X. D. Zhang and Y. Zhao, *Sol. Energy Mater. Sol. Cells*, 2011, **95**, 2126.
- 37 M. J. Wang, Y. Li, H. H. Huang, E. D. Peterson, W. Y. Nie, W. Zhou, W. Zeng, W. X. Huang, G. J. Fang, N. H. Sun, X. Z. Zhao and D. L. Carroll, *Appl. Phys. Lett.*, 2011, **98**, 103305.
- 38 S. Schumann, R. D. Campo, B. Illy, A. C. Cruickshank, M. A. McLachlan, M. P. Ryan, D. J. Riley, D. W. McCombb and T. S. Jones, *J. Mater. Chem.*, 2011, **21**, 2381.
- 39 N. Sekine, C. H. Chou, W. L. Kwan and Y. Yang, *Org. Electron.*, 2009, **10**, 1473.
- 40 M. Andersen, J. E. Carle, N. Cruys-Bagger, M. R. Lilliedal, M. A. Hammond, B. Winther-Jensen and F. C. Krebs, *Sol. Energy Mater. Sol. Cells*, 2007, **91**, 539.
- 41 R. Steim, S. A. Choulis, P. Schilinsky and C. J. Brabec, *Appl. Phys. Lett.*, 2008, **92**, 093303.
- 42 D. A. Rider, B. J. Worfolk, K. D. Harris, A. Lalany, K. Shahbazi, M. D. Fleischauer, M. J. Brett and J. M. Buriak, *Adv. Funct. Mater.*, 2010, **20**, 2404.
- 43 Q. D. Tai, X. Z. Zhao and F. Yan, *J. Mater. Chem.*, 2010, **20**, 7366.
- 44 B. Y. Yu, Y. Y. Chen, W. B. Wang, M. F. Hsu, S. P. Tsai, W. C. Lin, Y. C. Lin, J. H. Jou, C. W. Chu and J. J. Shyue, *Anal. Chem.*, 2008, **80**, 3412.
- 45 M. Wang, S. J. Moon, D. Zhou, F. L. Forman, N. L. Cevy-Ha, R. Humphry-Baker, C. Gratzel, P. Wang, S. M. Zakeeruddin and M. Gratzel, *Adv. Funct. Mater.*, 2010, **20**, 1821.
- 46 M. A. Lampert and P. Park, *Current injection in solids*, Academic Press, New York, 1970.